J. Fluid Mech. (1997), *vol.* 341, *pp.* 269–294. Printed in the United Kingdom

Axisymmetric free boundary problems

By MARK SUSSMAN[1]† AND PETER SMEREKA[2]

[1] Center for Computational Sciences and Engineering,
Lawrence Berkeley National Laboratory, Berkeley, CA 94720, USA

[2] Department of Mathematics, University of Michigan, Ann Arbor, MI 48109, USA

(Received 26 April 1996 and in revised form 7 February 1997)

We present a number of three-dimensional axisymmetric free boundary problems for two immiscible fluids, such as air and water. A level set method is used where the interface is the zero level set of a continuous function while the two fluids are solutions of the incompressible Navier–Stokes equation. We examine the rise and distortion of an initially spherical bubble into cap bubbles and toroidal bubbles. Steady solutions for gas bubbles rising in a liquid are computed, with favourable comparisons to experimental data. We also study the inviscid limit and compare our results with a boundary integral method. The problems of an air bubble bursting at a free surface and a liquid drop hitting a free surface are also computed.

1. Introduction

Axisymmetric free boundary problems have attracted considerable attention because they represent an excellent approximation to a number of important problems. For example, in situations with gravity there is often symmetry in the plane perpendicular to gravity; consequently the problem is reduced to only two space dimensions, namely elevation and radius. This is often found in experimental situations, such as an air bubble rising under gravity in water at moderate Reynolds numbers. This is in contrast to usual two-dimensional problems in which it is often difficult to find corresponding experimental conditions.

In this work we consider immiscible two-fluid flows such as water and air. We shall restrict ourselves to flows where the fluid velocity is much less than the speed of sound. This means we can approximate the fluids as incompressible. There has been considerable work done in this direction for axisymmetric flows. Ryskin & Leal (1984*a*, *b*) developed a method to compute the steady motion of a gas bubble rising in a liquid. Their method is based on constructing an orthogonal coordinate system which adjusts to fit the shape of the bubble. They confined their study to cases where the gas density and viscosity are much less than those of the fluid so that the motion of the gas could be neglected. A comparison of their work with the experimental work of Hnat & Buckmaster (1976) was excellent. Subsequently, Dandy & Leal (1989) extended this work to include the effects of the gas density and viscosity. In addition, they compared their results to the experiments of Thorsen, Stordalen & Terjesen (1968) and found excellent agreement.

A large body of work has focused on inviscid, incompressible axisymmetric flows where boundary integral methods are particularly adept. Miksis, Vanden-Broeck & Keller (1982) numerically deduced the shape of steadily rising bubbles using a

† Present address: University of California Davis, Davis, CA 95616, USA.

formulation similar to the one developed by Longuet-Higgins & Cokelet (1976). Baker, Meiron & Orszag (1984) developed a boundary integral method based on a dipole representation of the velocity potential which they applied to some axisymmetric problems. Lundgren & Mansour (1988) applied the method of Baker *et al.* to study liquid drop oscillations. Lundgren & Mansour (1991) extended the method to include toroidal geometry and studied vortex ring bubbles. Oguz & Prosperetti (1990) studied the impact of drops on liquid surfaces and the subsequent entrainment of an air bubble using a new boundary integral formulation. This work has important implications for the sound generated by rain. More recently, Boulton-Stone & Blake (1993) studied the problem of an air bubble bursting at a free surface. They included weak viscous effects in their computations in which they extended the formulation of Lundgren & Mansour (1988) by also considering the tangential component of the velocity due to the viscous boundary layer.

There is a significant amount of work which makes use of boundary integral formulations to study the collapse of an axisymmetric vapour bubble near a wall (see, for example, Best & Kucera 1992; Blake & Gibson 1987; or Blake, Taib & Doherty 1986). Due to the greater mobility of the flow away from the wall, the collapse of the bubble surface there proceeds at a greater speed than elsewhere, causing a jet to form and thread the bubble. The jet eventually penetrates the bubble completely, impacting the side of the bubble nearest the wall, causing the formation of a toroidal bubble. The interfacial structure of the bubble as it is transformed into a toroidal bubble is similar to that of an incompressible rising inviscid air bubble that eventually transforms into a vortex ring bubble (studied by Lundgren & Mansour (1991) and also studied in this paper). In the work of Best (1993) and Zhang, Duncan & Chahine (1993), the boundary integral method was extended in order to compute through the topology change. In both studies, the method used to handle the toroidal geometry was different from that of Lundgren & Mansour (1991).

Szymczak *et al.* (1993) have also studied the collapse of an axisymmetric vapour bubble near a wall. Like Best (1993) and Zhang *et al.*, they were able to compute through the topology change. Their approach used an Eulerian capturing scheme in which a one-sided density constraint is used to maintain the incompressibility of the liquid.

Nobari & Tryggvason (1994) have studied the coalescence of axisymmetric drops using a front-tracking/finite-difference scheme. An interesting feature of this work is that the Navier–Stokes equation is solved on a fixed grid with a front-tracking scheme to locate the interface. The method has been modified to allow the merging of fronts. It should also be pointed out that the above method was developed by Unverdi & Tryggvason (1992) who have done both two- and three-dimensional calculations. The method was extended to axisymmetric geometries by Jan & Tryggvason (1994) who used it to study the rise of surface-contaminated bubbles.

In this paper we offer another approach for computing free surface problems. We solve the Navier–Stokes equation in both fluids on a fixed grid as do Unverdi & Tryggvason and Szymczak *et al.* We 'capture' the front by defining the interface to be the zero level set of a continuous function which we shall call the level set function. Quantities such as density and viscosity which exhibit large jumps at the free surface depend on the level set function which is continuous across the free surface. The level set approach has been used for applications involving flow by mean curvature by Osher & Sethian (1988) and also for compressible multi-fluid flow applications by Mulder, Osher & Sethian (1992). The advantage of this approach is that topology changes present no difficulties; fronts can either merge or break up and no extra

coding is required. In our case we use the signed normal distance from the interface as the level set function. In the work of Sussman, Smereka & Osher (1994, henceforth referred to as Paper I), the level set approach was enhanced in order to compute two-dimensional free surface flows in which density and viscosity can have large jumps at the free surface and stiff surface tension effects can be included. In this paper we extend the results of Paper I to axisymmetric flows.

We examine several axisymmetric flow problems using the level set approach. We first study drop oscillations in a zero-gravity environment and find agreement with the theoretical results of Lamb (1932) and the numerical results of Lundgren & Mansour (1988). We also include steady solutions of gas bubbles rising in water, which are similar to the steady-state computations of Ryskin & Leal (1984*b*) and Dandy & Leal (1989). Our numerical results are similar to the experimental results of Hnat & Buckmaster (1976): our results for the rise speed differed by less than 5% from their findings.

The next series of free boundary problems presented share as a common feature the merging and/or break up of the interface We first study the rise and distortion of an initially spherical gas bubble in an initially still liquid. This problem has been studied in the inviscid limit by Lundgren & Mansour (1991). They show that the lower surface of the bubble will impact its upper surface causing the formation of a toroidal bubble. They do not, however, study the details after impact. We study the formation of the toroidal bubble using the level set method and find excellent agreement with Lundgren & Mansour before the time of impact. The level set approach allows us to compute the flow through the impact. In order to validate the results of this computation we also use a boundary integral method that allows for the topology change. We find good agreement between these two approaches.

We next study the impact of a liquid drop on the free surface of the same liquid. This problem is very important in the understanding of underwater noise created by rain. Pumphrey & Crum (1988) have experimentally verified that a raindrop can cause an air bubble to be formed in the water. Oguz & Prosperetti (1990) have studied this problem numerically; for initial conditions, they considered the raindrop to be physically connected to the free surface. Using the level set approach we found reasonable agreement with the results of Oguz & Prosperetti and Pumphrey & Crum.

Finally, we study the problem of a gas bubble rising due to gravity through a liquid and ultimately bursting at a liquid–gas interface. This problem has been studied by Boulton-Stone & Blake (1993) using a boundary integral method. They chose initial conditions so that the bubble is already connected to the free surface in a manner similar to Oguz & Prosperetti (1990). We are able to study the impact of the air bubble on the free surface using the level set method. We compute results for a bubble that initially is fully submerged.

2. Level set formulation

2.1. *Governing equations*

To fix ideas we shall call one of the fluids a liquid and the other a gas. We assume that both fluids are governed by the incompressible Navier–Stokes equation; therefore,

$$\left.\begin{aligned} \rho_\ell \frac{\mathrm{D}\boldsymbol{u}_\ell}{\mathrm{D}t} &= -\nabla p_\ell + 2\mu_\ell \nabla\cdot\mathscr{D} + \rho_\ell \boldsymbol{g}, \quad \nabla\cdot\boldsymbol{u}_\ell = 0, \quad \boldsymbol{x}\in \text{the liquid},\\ \rho_g \frac{\mathrm{D}\boldsymbol{u}_g}{\mathrm{D}t} &= -\nabla p_g + 2\mu_g \nabla\cdot\mathscr{D} + \rho_g \boldsymbol{g}, \quad \nabla\cdot\boldsymbol{u}_g = 0, \quad \boldsymbol{x}\in \text{the gas}, \end{aligned}\right\} \tag{1}$$

where $\boldsymbol{u}$ is the velocity, p is the pressure, ρ is the density, and μ is the viscosity of the fluid. The subscripts ℓ and g denote the liquid and the gas phase, respectively. $\mathrm{D}/\mathrm{D}T$ is the material derivative, $\mathscr{D}$ is the rate of deformation tensor, and $\boldsymbol{g}$ is the acceleration due to gravity. The boundary conditions at the interface, Γ, between the phases are

$$(2\mu_\ell \mathscr{D} - 2\mu_g \mathscr{D}) \cdot \boldsymbol{n} = \left(p_\ell - p_g + \sigma\kappa\right) \boldsymbol{n} \quad \text{and} \quad \boldsymbol{u}_\ell = \boldsymbol{u}_g, \quad \boldsymbol{x} \in \Gamma, \tag{2}$$

where $\boldsymbol{n}$ is the unit normal to the interface drawn outwards from the gas to the liquid, $\kappa = \nabla \cdot \boldsymbol{n}$ is the curvature of the interface, and σ is the coefficient of surface tension.

We will denote the domain containing the two fluids as Ω and its boundary as $\partial\Omega$. Since the fluid cannot penetrate the boundary, we have

$$\boldsymbol{u} \cdot \boldsymbol{n} = 0 \qquad \text{on} \qquad \partial\Omega. \tag{3}$$

Our main interest is the free boundary between the two fluids and not the boundary layer at the solid wall ($\partial\Omega$). To suppress the formation of vorticity at the wall we use the free-slip boundary condition

$$\boldsymbol{n} \cdot \nabla \boldsymbol{u} = 0 \qquad \text{on} \qquad \partial\Omega. \tag{4}$$

Note: condition (3) implies that we only consider bubbles of constant volume and cannot consider bubbles that grow in size due to a decrease in hydrostatic pressure.

2.2. *Level set function*

In our algorithm the interface, Γ, is the zero level set of ϕ:

$$\Gamma = \{\boldsymbol{x} | \phi(\boldsymbol{x}, t) = 0\}.$$

We also take $\phi < 0$ in the gas region and $\phi > 0$ in the liquid region. Hence, we have

$$\phi(\boldsymbol{x}, t) \quad \begin{cases} > 0 & \text{if } \boldsymbol{x} \in \text{the liquid} \\ = 0 & \text{if } \boldsymbol{x} \in \Gamma \\ < 0 & \text{if } \boldsymbol{x} \in \text{the gas.} \end{cases} \tag{5}$$

The unit normal on the interface, drawn from the gas into the liquid, and the curvature of the interface can easily be expressed in terms of $\phi(\boldsymbol{x}, t)$:

$$\boldsymbol{n} = \left.\frac{\nabla\phi}{|\nabla\phi|}\right|_{\phi=0} \quad \text{and} \quad \kappa = \nabla \cdot \left.\left(\frac{\nabla\phi}{|\nabla\phi|}\right)\right|_{\phi=0}. \tag{6}$$

Next, we let

$$\boldsymbol{u} = \begin{cases} \boldsymbol{u}_\ell, & \phi > 0 \\ \boldsymbol{u}_g, & \phi \leqslant 0, \end{cases}$$

where $\boldsymbol{u}$ is called the fluid velocity. By virtue of the boundary conditions, $\boldsymbol{u}$ is continuous across the interface. Since the interface moves with the fluid particles, the evolution of ϕ is then given by

$$\frac{\partial\phi}{\partial t} + \boldsymbol{u} \cdot \nabla\phi = 0. \tag{7}$$

It was demonstrated by Osher & Sethian (1988) and Evans & Spruck (1991), for the case when $\boldsymbol{u}$ is prescribed by the mean curvature of the front, that equation (7) accurately moves the zero level set according to $\boldsymbol{u}$ even through the merging and breaking up of fluid mass. To better understand equation (7), we can use ideas from

the method of characteristics. Assume that at time t, the interface Γ is parameterized by $(x(s,t), y(s,t))$, then the evolution of (x, y) is determined by the equations

$$\frac{\mathrm{d}x(s,t)}{\mathrm{d}t} = u(x(s,t), y(s,t)),$$
$$\frac{\mathrm{d}y(s,t)}{\mathrm{d}t} = v(x(s,t), y(s,t)).$$

Since $\phi(x(s,t), y(s,t), t)$ is defined to be zero for all (s,t), we must have

$$\frac{\mathrm{d}\phi(x(s,t), y(s,t), t)}{\mathrm{d}t} \equiv \frac{\mathrm{d}\phi}{\mathrm{d}x}\frac{\mathrm{d}x}{\mathrm{d}t} + \frac{\mathrm{d}\phi}{\mathrm{d}y}\frac{\mathrm{d}y}{\mathrm{d}t} + \frac{\mathrm{d}\phi}{\mathrm{d}t} = \phi_t + u\phi_x + v\phi_y = 0.$$

The governing equation for the fluid velocity, $\boldsymbol{u}$, along with the boundary conditions can be written as a single equation:

$$\rho(\phi)\frac{\mathrm{D}\boldsymbol{u}}{\mathrm{D}t} = -\nabla p + \nabla \cdot (2\mu(\phi)\mathscr{D}) - \sigma\kappa(\phi)\delta(\phi)\nabla\phi + \rho(\phi)\boldsymbol{g}, \tag{8}$$

where ρ and μ are, respectively, the density and viscosity and δ is the Dirac delta function. The surface tension force is interpreted as a body force localized on the interface. By $\kappa(\phi)$ we mean

$$\kappa(\phi) = \nabla \cdot \left(\frac{\nabla\phi}{|\nabla\phi|}\right).$$

Since the density and viscosity are constant in each fluid, they take two different values depending on the sign of ϕ; hence we write

$$\rho(\phi) = \rho_g + (\rho_\ell - \rho_g)H(\phi) \tag{9}$$

and

$$\mu(\phi) = \mu_g + (\mu_\ell - \mu_g)H(\phi), \tag{10}$$

where $H(\phi)$ is the Heaviside function given by

$$H(\phi) = \begin{cases} 0 & \text{if } \phi < 0 \\ \frac{1}{2} & \text{if } \phi = 0 \\ 1 & \text{if } \phi > 0. \end{cases}$$

The Navier–Stokes equation for two-fluid flows was written in similar form and used by Unverdi & Tryggvason (1992). The fact that the surface tension can be written as a delta function concentrated at the interface has been used by Unverdi & Tryggvason (1992) and Brackbill, Kothe, & Zemach (1992). The form we use here is due to Chang *et al.* (1995). The derivation of equation (8) can be found in Chang *et al.* in which it is shown that the formulation of (8) admits solutions which are consistent with the free-surface boundary conditions (2).

2.3. *Dimensionless form*

It is useful to write (8) in dimensionless form using the following dimensionless variables:

$$\boldsymbol{x} = L\boldsymbol{x}', \ \boldsymbol{u} = U\boldsymbol{u}', \ t = (L/U)t', \ p = p'\rho_\ell U^2, \ \rho = \rho_\ell\rho', \text{ and } \mu = \mu_\ell\mu',$$

where the primes denote dimensionless variables. If we substitute these variables into (8) and drop the primes, we have

$$\boldsymbol{u}_t + \nabla p/\rho(\phi) = \boldsymbol{F}, \tag{11}$$

where

$$\boldsymbol{F} = -\boldsymbol{u}\cdot\nabla\boldsymbol{u} - \frac{\boldsymbol{z}}{Fr} + \frac{1}{\rho(\phi)}\left(\frac{1}{Re}\nabla\cdot(2\mu(\phi)\mathscr{D}) - \frac{1}{We}\kappa(\phi)\delta(\phi)\nabla\phi\right), \tag{12}$$

and $\boldsymbol{z}$ is a unit vector in the z-direction. The density and viscosity are now

$$\rho(\phi) = \lambda + (1-\lambda)H(\phi) \quad \text{and} \quad \mu(\phi) = \eta + (1-\eta)H(\phi), \tag{13}$$

where $\lambda = \rho_g/\rho_\ell$ is the density ratio and $\eta = \mu_g/\mu_\ell$ is the viscosity ratio. The dimensionless groups used above are the Reynolds number,

$$Re = \rho_\ell LU/\mu_\ell,$$

the Froude number,

$$Fr = U^2/gL,$$

and the Weber number,

$$We = \rho_\ell LU^2/\sigma.$$

We shall also use the Bond number

$$B = \rho_\ell gL^2/\sigma = We/Fr.$$

2.4. *Axisymmetric flows*

In this paper we consider only axisymmetric flows; therefore $\boldsymbol{x} = (r,z)^T$, where r is the radial coordinate and z is vertical coordinate. Let $\nabla_c = (\partial_r, \partial_z)^T$ and $\nabla_c^\perp = (\partial_z, -\partial_r)^T$. The restriction to axisymmetric flows offers some simplification as the velocity, $\boldsymbol{u} = (u_r, u_z)^T$, can be deduced by a stream function. Thus it follows that

$$\boldsymbol{u} = (1/r)\nabla_c^\perp\psi. \tag{14}$$

If we substitute (14) into the $\boldsymbol{u}_t$ term of (11), multiply by $\rho(\phi)$, and apply $\nabla_c^\perp\cdot$ to both sides, the pressure term is eliminated. This gives the following variable-coefficient Poisson equation for ψ_t on Ω:

$$\nabla_c\cdot\left(\frac{\rho(\phi)}{r}\nabla_c\psi_t\right) = \nabla_c^\perp\cdot(\rho(\phi)\boldsymbol{F}), \tag{15}$$

with boundary conditions

$$\psi_t = 0 \quad \text{for} \quad \boldsymbol{x}\in\partial\Omega. \tag{16}$$

These boundary conditions follow since the normal velocity of $\boldsymbol{u}$ must vanish on the boundary. In our numerical computations we will take

$$\Omega = \{(r,z)|0\leqslant r\leqslant R \text{ and } 0\leqslant z\leqslant H\},$$

where R and H are the radius and height of the domain.

The axisymmetric Navier–Stokes equations for two incompressible immiscible fluids in level set form are given by (7), (13), (14), and (15).

2.5. *Thickness of the interface*

In order to solve (15) numerically we must modify it slightly due to the sharp changes in ρ across the front and also because of the numerical difficulties presented by the Dirac delta function contained in $\boldsymbol{F}$. To alleviate these problems we shall give the interface a fixed thickness that is proportional to the spatial mesh size. This allows us to replace $\rho(\phi)$ by a smoothed density, $\rho_\varepsilon(\phi)$, which is given by

$$\rho_\varepsilon(\phi) = \lambda + (1-\lambda)H_\varepsilon(\phi), \tag{17}$$

with

$$H_\varepsilon(\phi) = \begin{cases} 0 & \text{if } \phi < -\varepsilon \\ \frac{1}{2}[1 + \phi/\varepsilon + (1/\pi)\sin(\pi\phi/\varepsilon)] & \text{if } |\phi| \leqslant \varepsilon \\ 1 & \text{if } \phi > \varepsilon. \end{cases} \tag{18}$$

The smoothed or mollified delta function is

$$\delta_\varepsilon(\phi) = \frac{\mathrm{d}H_\varepsilon}{\mathrm{d}\phi}. \tag{19}$$

It is clear from (18) that the thickness of the interface is approximately

$$2\varepsilon/|\nabla\phi|. \tag{20}$$

In our algorithm the front will have a uniform thickness, consequently we must have $|\nabla\phi| = 1$ when $|\phi| \leqslant \varepsilon$. A function that satisfies

$$|\nabla d| = 1 \quad \text{for} \quad \boldsymbol{x} \in \Omega \quad \text{with} \quad d = 0 \quad \text{for} \quad \boldsymbol{x} \in \Gamma \tag{21}$$

is called a distance function. This is because d is the signed normal distance to the interface, Γ.

If a level set function is equal to a distance function it then follows from (18) that the thickness of the interface is 2ε. In our numerical calculations we shall take $\varepsilon = \alpha\Delta x$ where Δx is the grid size. Therefore, the interface will reduce in thickness as we refine our mesh.

Therefore it seems ideal to choose the level set function to be a distance function. It is clear that we can choose $\phi(\boldsymbol{x}, 0)$ to be a distance function; however, under the evolution of (7) it will not necessarily remain as such. We must then be able to solve the following problem: given a level set function, $\phi(\boldsymbol{x})$, reinitialize it to be a distance function *without changing its zero level set*. This can be achieved by solving the following partial differential equation:

$$\frac{\partial d}{\partial \tau} = \mathrm{sign}(\phi)(1 - |\nabla d|), \tag{22}$$

with initial conditions

$$d(\boldsymbol{x}, 0) = \phi(\boldsymbol{x}),$$

where

$$\mathrm{sign}(\phi) = \begin{cases} -1 & \text{if } \phi < 0 \\ 0 & \text{if } \phi = 0 \\ 1 & \text{if } \phi > 0 \end{cases} \tag{23}$$

and τ is an artificial time. The steady solutions of (22) are distance functions. Furthermore, since $\mathrm{sign}(0) = 0$, $d(\boldsymbol{x}, \tau)$ has the same zero level set as $\phi(\boldsymbol{x})$. Therefore we simply solve (22) to steady state and then replace $\phi(\boldsymbol{x})$ by $d(\boldsymbol{x}, \tau_{steady})$. It is clear from (18) that we need only ϕ to be a distance function close to the front. We have then reached 'steady state' when

$$|\nabla d| = 1 \quad \text{for} \quad |d| \leqslant \varepsilon.$$

A nice feature of using this procedure is that the level set function is first reinitialized near the front. To see this we rewrite (22) as

$$d_\tau + \boldsymbol{w} \cdot \nabla d = \mathrm{sign}(\phi) \tag{24}$$

where

$$\boldsymbol{w} = \mathrm{sign}(\phi)\nabla d/|\nabla d|.$$

It is evident that (24) is a nonlinear hyperbolic equation with the characteristic velocities pointing *outwards* from the interface in the direction of the normal. Thus d will be first reinitialized to $|\nabla d| = 1$ near the interface. Since we need the level set function only to be a distance function near the interface, it is not necessary to solve (24) to steady state over the whole domain. This indicates that only a fixed number of iterations are necessary in order to ensure that the level set function is a distance function near the interface. For example, if the iteration step size is $\Delta\tau$ and the total interfacial thickness is 2ε, we can stop the iteration process after no more than $\varepsilon/\Delta\tau$ time steps. In practice we find that we need only two or three iterations as we are already close to the distance function.

2.6. *Numerical procedure*

The details of the numerical procedure can be found in Paper I. The modifications for the axisymmetric geometry are straightforward and can be found in Sussman (1994). For the convenience of the reader we outline the basic numerical algorithm along with improvements of the method.

2.6.1. *Numerical algorithm*

Step 1. Initialize $\phi(\boldsymbol{x}, 0)$ to be the signed normal distance to the front. Initialize $\boldsymbol{u}(\boldsymbol{x}, 0)$ to be the initial divergence-free velocity (identically zero in our case).

Step 2. Compute $\boldsymbol{F}$ by replacing $\delta(\phi)$ by $\delta_\varepsilon(\phi)$ and $H(\phi)$ by $H_\varepsilon(\phi)$ in (12).

Step 3. Solve the Poisson equation (15) for ψ_t and compute a new $\boldsymbol{u}_t$. Use this to update $\boldsymbol{u}$; denote the updated $\boldsymbol{u}$ as $\boldsymbol{u}^{n+1}$.

Step 4. Update the location of the interface by solving (7) for one time step using $\boldsymbol{u}^{n+1}$. Denote the updated value of ϕ by $\phi^{n+1/2}$.

Step 5. Reinitialize $\phi^{n+1/2}$ by solving

$$\phi_\tau = S_\varepsilon(\phi^{n+1/2})(1 - |\nabla\phi|) \quad \text{with} \quad \phi(\boldsymbol{x}, 0) = \phi^{n+1/2}(\boldsymbol{x})$$

to 'steady state'. Here S_ε is a smoothed version of (23). We denote this solution by ϕ^{n+1}. By steady state we mean that $|\nabla\phi| = 1 + O(\Delta x)$ for $|\phi| < \varepsilon$ (as noted previously $\varepsilon = \alpha\Delta x$ and typically α is 2).

Step 6. We have now advanced one time step. The zero level set of ϕ^{n+1} gives the new interface position and it is a distance function close to the front. One then proceeds back to step 2.

Evidence was provided in Paper I to show that the numerical scheme converged in a number of different applications. We have performed similar tests for the axisymmetric case but chose not to present them here for the sake of brevity. In the numerical calculations presented in §4 the mesh is sufficiently refined so that the numerical method has converged.

2.6.2. *Improvements*

We have made several improvements of the level set method described in Paper I to increase accuracy and stability. We use a third-order ENO method as developed by Shu & Osher (1989) for differencing the advective terms. We also use a second-order Runge–Kutta method to advance in time as opposed to the second-order Adam–Bashforth scheme used in Paper I. Finally, we use an improvement in the

reinitialization step which was developed by Fatemi & Sussman (1995) in order to increase its accuracy.

We will now briefly discuss the modification to the reinitialization step. We interpret the term, sign(ϕ), in equation (22) as a 'constraint' used both to prevent the interface from moving and also to implicitly prescribe boundary conditions at the interface. For discretization purposes we wish to enforce another constraint: the volume filled by each fluid must stay constant throughout the reinitialization. For each cell, Ω_{ij}, we define volume as

$$V_{ij}^n = \int_{\Omega_{ij}} H(\phi^n) r \mathrm{d}r\mathrm{d}z, \tag{25}$$

where H is the Heaviside function described below equation (10) and ϕ^n is the value of ϕ at τ_n, the 'time' after the nth iteration in the reinitialization step.

Because volume should not change, we should have $V_{ij}^n = V_{ij}^0$. Nevertheless, if the reinitialization step slightly changes the location of the zero level set, we then have, for $\tau_n - \tau_0 = O(\Delta x)$,

$$\begin{aligned} V_{ij}^n - V_{ij}^0 &\approx (\tau_n - \tau_0) \int_{\Omega_{ij}} \frac{\mathrm{d}H_\varepsilon(\phi^0)}{\mathrm{d}\tau} r\mathrm{d}r\mathrm{d}z \\ &= \int_{\Omega_{ij}} \frac{\mathrm{d}H_\varepsilon(\phi_0)}{\mathrm{d}\phi}(\phi^n - \phi^0) r\mathrm{d}r\mathrm{d}z, \end{aligned} \tag{26}$$

where

$$\frac{\mathrm{d}H_\varepsilon}{\mathrm{d}\phi} = \begin{cases} 0 & \text{if } |\phi| > \varepsilon \\ \frac{1}{2}[(1/\varepsilon) + (1/\varepsilon)\cos(\pi\phi/\varepsilon)] & \text{if } |\phi| \leqslant \varepsilon. \end{cases} \tag{27}$$

In order to minimize volume variation, we project the current values of the level set function, denoted as $\widetilde{\phi_{ij}^n}$, onto new values, denoted as ϕ_{ij}^n, which satisfy

$$\int_{\Omega_{ij}} \frac{\mathrm{d}H_\varepsilon(\phi^0)}{\mathrm{d}\phi}(\phi^n - \phi^0) r\mathrm{d}r\mathrm{d}z = 0. \tag{28}$$

If (28) is satisfied then by (26) the volume change will be very small. To implement this projection we assume ϕ_{ij}^n has the form,

$$\phi_{ij}^n = \widetilde{\phi_{ij}^n} + \lambda_{ij}(\tau_n - \tau_0)\frac{\mathrm{d}H_\varepsilon(\phi^0)}{\mathrm{d}\phi}, \tag{29}$$

where λ_{ij} is assumed constant in Ω_{ij}. After substituting (29) into (28), we have

$$\lambda_{ij} = \frac{-\displaystyle\int_{\Omega_{ij}} \frac{\mathrm{d}H_\varepsilon(\phi_0)}{\mathrm{d}\phi}\left(\frac{\widetilde{\phi^n} - \phi^0}{\tau_n - \tau_0}\right) r\mathrm{d}r\mathrm{d}z}{\displaystyle\int_{\Omega_{ij}} \left(\frac{\mathrm{d}H_\varepsilon(\phi^0)}{\mathrm{d}\phi}\right)^2 r\mathrm{d}r\mathrm{d}z}. \tag{30}$$

Equation (30) is discretized in each cell by using a nine-point stencil to perform the integration. Since λ_{ij} is assumed constant in each cell, (30) can be solved both explicitly and quickly. The projection step given by (29) is applied after each reinitialization step. In our work we have found that the above constraint helps ϕ converge to a distance function while still maintaining the original zero level set.

2.6.3. *Far-field boundary conditions*

Many experimental situations occur in large domains. Due to limited computing resources it is not possible to compute in domains of this size. In certain situations, the velocity field decays to zero sufficiently fast in space so that it is still possible to compare with experiments even when the computational domain is small. There are, however, situations where the effects of a small computational domain make comparison with experiments difficult. In these cases it is expedient to modify the scheme near the boundary to produce 'far-field' boundary conditions.

We still enforce zero normal velocity at the boundary, but assume that the cells, Ω_{ij}, which touch the wall, have dimensions of $M \times \Delta x$ as opposed to $\Delta x \times \Delta x$. The difference formulas in the advection and projection steps are then modified accordingly. The constant, M, can be specified to be as large as necessary, as long as the tangential velocity does not change much in the direction normal to the boundary. For a gas bubble that attains a steady state (see figure 4), the expected steady rise speed matches experimental findings within 5% when our far-field boundary conditions are used. Without the far-field boundary conditions, wall effects would cause the steady rise speed to be 14% slower than the expected value.

3. Boundary integral method

In this section, we will study the motion of gas-filled bubbles in an incompressible inviscid liquid using a boundary integral method. The basic formulation of the method is due to Baker *et al.* (1984). Their method has been modified by Lundgren & Mansour (1991) to account for toroidal geometry. We will outline this method and provide an alternative modification for the toroidal geometry.

The liquid outside the bubble is taken to be irrotational; therefore, its velocity, $\boldsymbol{u}$, is given by

$$\boldsymbol{u} = \nabla\phi, \quad \text{where} \quad \nabla^2\phi = 0. \tag{31}$$

Because we are considering incompressible flows, this allows the velocity potential, ϕ, to be represented by a distribution of dipoles on the bubble interface. This is given by

$$\phi(\boldsymbol{r}) = \int_\Gamma \mu(\boldsymbol{r}')\boldsymbol{n}(\boldsymbol{r}') \cdot \nabla' g(\boldsymbol{r} - \boldsymbol{r}')\mathrm{d}S, \tag{32}$$

where μ is the dipole density and

$$g(\boldsymbol{r} - \boldsymbol{r}') = -\frac{1}{4\pi|\boldsymbol{r} - \boldsymbol{r}'|}$$

is the Green's function for the Laplacian in R^3. The unit normal, $\boldsymbol{n}$, is taken outward from the liquid into the bubble. The beauty of the boundary integral approach is that the entire solution can be deduced using information on the boundary. To deduce the liquid velocity on the boundary, we first take the limit of (32) as the point, $\boldsymbol{r}$, tends to the bubble surface. This limit is

$$\phi_s = \tfrac{1}{2}\mu(\boldsymbol{r}) + \fint_\Gamma \mu(\boldsymbol{r}')\boldsymbol{n}(\boldsymbol{r}') \cdot \nabla' g(\boldsymbol{r} - \boldsymbol{r}')\mathrm{d}S, \tag{33}$$

where ϕ_s is the velocity potential on the bubble surface and $\fint$ denotes the principal value. Strictly speaking, the principal value is not necessary since the singularity is integrable; however, we keep it to remind us that the integrand is singular. It is clear that the tangential components of the velocity can be found from surface derivatives

of ϕ_s. We introduce a vector potential, $\boldsymbol{A}$, to find the normal component of the velocity. $\boldsymbol{A}$, evaluated on the surface, is

$$\boldsymbol{A} = \fint_{\Gamma} \mu(\boldsymbol{r}')\boldsymbol{n}(\boldsymbol{r}') \times \nabla' g(\boldsymbol{r} - \boldsymbol{r}')\mathrm{d}S. \tag{34}$$

Here the principal value is necessary. It follows that

$$\boldsymbol{u} \cdot \boldsymbol{n} = (\boldsymbol{n} \times \nabla) \cdot \boldsymbol{A}, \tag{35}$$

and only requires surface derivatives to evaluate. With the velocity of liquid at the surface of the bubble known, the motion of the interface is determined by

$$\mathrm{d}\boldsymbol{r}/\mathrm{d}t = \boldsymbol{u}. \tag{36}$$

The time evolution of the velocity potential is determined by Bernoulli's equation,

$$\partial\phi/\partial t + \tfrac{1}{2}|\boldsymbol{u}|^2 + p/\rho + gz = p_\infty/\rho, \tag{37}$$

where ρ is the liquid density, z is the vertical coordinate, g is the acceleration due to gravity, and p_∞ is the ambient pressure at $z = 0$. The jump in pressure across the bubble surface must be balanced by surface tension; therefore

$$p_s - p_s^{(b)} = \sigma \nabla \cdot \boldsymbol{n},$$

where p_s is the pressure on the liquid side of the interface and $p_s^{(b)}$ is the pressure on the gas side; σ is the surface tension coefficient and $\nabla \cdot \boldsymbol{n}$ is the curvature of the interface. If we assume that the pressure in the bubble is spatially homogeneous we can then combine the above equations to find the time evolution of

$$\mathrm{d}\phi_s/\mathrm{d}t - \tfrac{1}{2}|\boldsymbol{u}|^2 + \sigma/\rho + gz = (p_\infty - p_b(t))/\rho; \tag{38}$$

$p_b(t)$ is the pressure in the gas bubble whose time dependence is determined so as to keep the volume of the bubble fixed. It is clear that p_b will only change ϕ_s by a constant amount which will not affect $\boldsymbol{u}$. Therefore it is unnecessary to determine p_b and the right-hand side of (38) can be set to zero. The procedure to solve this system numerically is as follows: initially we know ϕ, so we solve (33) iteratively for μ. Simple iteration will not work since

$$\fint_{\Gamma} \boldsymbol{n}(\boldsymbol{r}') \cdot \nabla' g(\boldsymbol{r} - \boldsymbol{r}')\mathrm{d}S = -\tfrac{1}{2};$$

thus (33) is only unique up to a constant. To remove this difficulty we can add a constraint to (33) such as $\mu(0) = 0$. With μ known, we use (34) to determine the normal velocity. The tangential velocity is determined from ϕ; the velocity potential is updated with Bernoulli's equation and the interface position is updated with (36). With the velocity potential and interface position updated we repeat the steps above (for details on the numerical implementation, see Lundgren & Mansour 1988).

3.1. *Modification for toroidal geometry*

We observe that the bottom of the bubble can touch its top. When the bubble pinches it has a toroidal shape and the liquid domain is no longer simply connected. Therefore the velocity potential is cyclic or multiple-valued. To ensure a unique solution the circulation (C) around the bubble must be specified; once specified it will remain constant.

In this case we modify (32) in the fashion suggested by Lundgren & Mansour (1991):

$$\phi = \phi' + \phi_b, \tag{39}$$

where

$$\phi(\boldsymbol{r}) = \oint_\Gamma \mu(\boldsymbol{r}')\boldsymbol{n}(\boldsymbol{r}') \cdot \nabla' g(\boldsymbol{r} - \boldsymbol{r}')\mathrm{d}S$$

and

$$\phi_b(\boldsymbol{r}) = C \int_B \boldsymbol{n}(\boldsymbol{r}') \cdot \nabla' g(\boldsymbol{r} - \boldsymbol{r}')\mathrm{d}S.$$

Here B is an artificial barrier and must terminate strictly inside the bubble; ϕ' is a single-valued velocity potential, whereas ϕ_b is a cyclic velocity potential with a jump of C across B; ϕ_b is the velocity potential of the vortex ring located on the boundary of B. It is expedient, for numerical reasons, to keep the location of this ring as far from the bubble interface as possible. An expression for ϕ_b is given in Lamb (1932, §161), although here we use the above form for numerical computation. In a similar fashion, we can write the vector potential as

$$\boldsymbol{A} = \oint_\Gamma \mu(\boldsymbol{r}')\boldsymbol{n}(\boldsymbol{r}') \times \nabla' g(\boldsymbol{r} - \boldsymbol{r}')\mathrm{d}S + C\psi_b\boldsymbol{\theta},$$

where ψ_b is the stream function for a vortex ring and $\boldsymbol{\theta}$ is a unit vector in the θ-direction (Lamb 1932, §161). The procedure used here is basically the same as that used in the simply connected case. We use the above equations to compute the velocity and use (36) and (37) to update the velocity potential and interface. As pointed out by Lundgren & Mansour(1991), the fluid particles at the boundary must not cross the barrier during a partial time step. To remove this possibility we simply advect the barrier with the fluid particles on the boundary. Without modification, the edge of the barrier can become very close to the bubble interface; therefore we periodically reposition the barrier so that its edge is not close to the interface. Lundgren & Mansour present a different solution which ultimately has the centre of the vortex ring at the centre of mass of the bubble. We tried the approach outlined by Lundgren & Mansour and obtained identical results. The disadvantage of their approach is that the centre of mass can be a bad location for the vortex ring. The disadvantage of our approach is that we need to explicitly determine the velocity potential of the vortex ring. Best (1993) also offers a method for computing in the toroidal geometry; rather than keep the barrier a disc he chooses to advect the entire barrier with the fluid. More recently, Best (1994) keeps the barrier a disc.

3.2. *Implementation of the topology change*

The numerical calculations of Lundgren & Mansour (1991) show an incompressible gas bubble rising under gravity in an irrotational liquid. When the bubble is initially spherical and the surface tension is sufficiently small, they find that the bottom surface of the bubble will collide with its upper surface at a single point. As postulated by Benjamin & Ellis (1966, see also Benjamin 1987), this will give rise to a toroidal bubble with circulation. The circulation will be equal to the difference of velocity potentials between the two colliding points on the bubble surface. This postulate was used by Lundgren & Mansour (1991) to estimate the circulation around a toroidal bubble. They went on to compute the motion of a toroidal bubble; the initial condition was a torus with a circular cross-section. They did not, however, explore the details occurring immediately after collision.

Best (1993) considered the collapse of a compressible gas bubble and the details of the topology change. He utilized the concept of pressure impulse to show that the velocity potential on the surface of the bubble would not change for points that did not collide and that the circulation could be determined using the postulate of Benjamin & Ellis (1966). He used this argument to develop a numerical algorithm to integrate the bubble through the topology change. The fundamental difficulty with this approach is that the topology change has to be implemented by numerical 'surgery'. Briefly, this is done as follows: first, one integrates the equations of motion until the lower surface gets as close as possible to the upper surface (the singular nature of the kernel in (33) prevents integration to the collision time). Next, one removes the two points on the axis of symmetry and 'connects' the upper and lower surfaces using some sort of numerical interpolation (we use cubic splines). In our calculations we implement this 'surgery' in a manner very similar to the approach taken by Best (1993). Although a reasonable approach, it should be emphasized that it is arbitrary. In the level set method the thickness parameter is also arbitrary. However, our studies indicate that our results are not sensitive to this parameter.

4. Results

4.1. *Zero-gravity liquid drops*

4.1.1. *Linear motion*

We now compute zero-gravity drop dynamics and compare these with the linearized drop oscillation solutions of Lamb (1932). The interfacial position of the drop is shown to be

$$r(\theta, t) = a + \epsilon P_n(\cos(\theta)) \sin(\omega_n t),$$

where

$$\omega_n^2 = \frac{1}{We} \frac{n(n-1)(n+1)(n+2)}{a^3(n+1+n\lambda)} \tag{40}$$

and P_n is the Legendre polynomial of order n. This equation is written in dimensionless form (the solution can be found in Lamb 1932, §275). If viscosity is present, the amplitude is proportional to $\exp(-t/\tau)$, where

$$\tau = \frac{a^2 Re}{(2n+1)} \left(\frac{n + \lambda(n+1)}{n(n-1) + \eta(n+1)(n+2)} \right). \tag{41}$$

This equation is derived following the approach outlined in Lamb (1932, §355).

We compute the evolution of a drop with $a = 1$, $Fr = \infty$, $Re = 200$, $We = 2$, $\lambda = 0.01$, and $\eta = 0.01$. The initial interface is given by $r(\theta, 0)$, with $\varepsilon = 0.02$ and $n = 2$. With these parameters we find $\omega_2 = 2.00$ and $\tau = 38.3$. The fluid domain is $\Omega = \{(r, z) | 0 \leqslant r \leqslant 1.5 \text{ and } 0 \leqslant z \leqslant 3\}$ and the grid size is 50×100. The results of our computation are shown in figure 1 where we display $r(0, t)$ and compare it with the expected linearized viscous effects. The average dimensionless period is 3.18 and the expected linearized period is 3.14.

4.1.2. *Nonlinear motion*

For our second test, we compute large-amplitude oscillations and compare these with the results of Lundgren & Mansour (1988). We compute the evolution of a drop with $Fr = \infty$, $Re = 2000$, $W = 2$, $\lambda = 0.01$, and $\eta = 0.01$. The initial interface is given by $r(\theta, 0)$, with $\varepsilon = 0.3$ and $n = 4$. The fluid domain is $\Omega = \{(r, z) | 0 \leqslant r \leqslant 2$

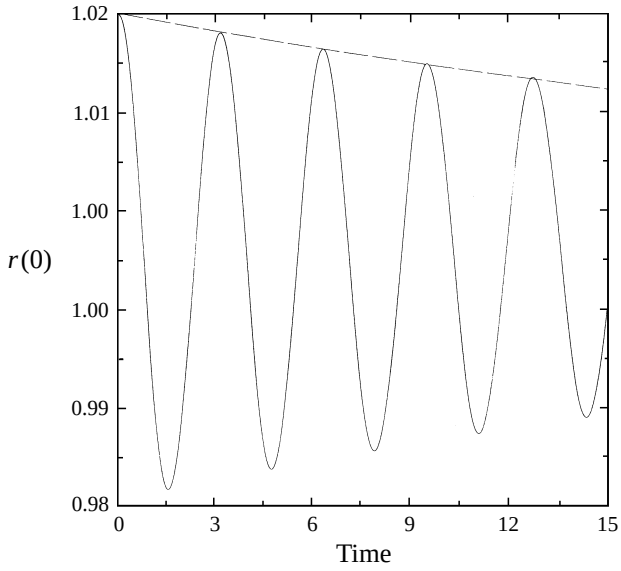

FIGURE 1. Motion of a viscous drop in zero gravity with $\lambda = 0.01$, $\eta = 0.01$, $Re = 200$, $We = 2$, and $Fr = \infty$: the time evolution of $r(0, t)$ initialized with P_2 shape (the solid curve) along with the predicted viscous envelope (the dashed curve).

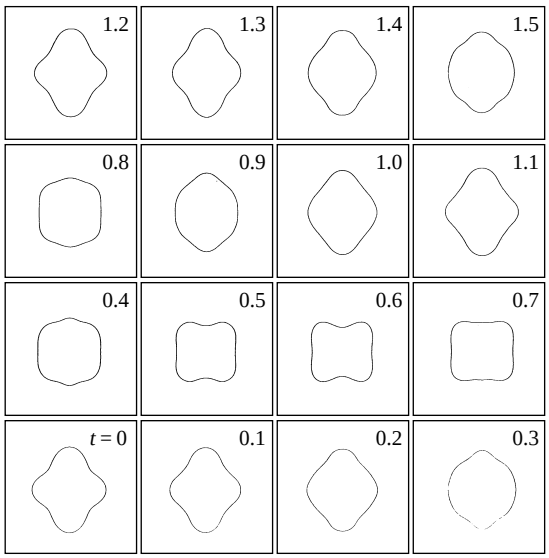

FIGURE 2. Motion of a viscous drop in zero gravity with $\lambda = 0.01$, $\eta = 0.01$, $Re = 2000$, $We = 2$, and $Fr = \infty$: the shape oscillations when the drop is initialized with a P_4 shape.

and $0 \leqslant z \leqslant 4\}$ and the grid size is 64×128. In figure 2, we display the drop shape from $t = 0$ to $t = 1.6$. In figure 3, we compare results at $t = 1.1$ using the level set method to corresponding results computed by Lundgren & Mansour (1988, see figure 6) using the boundary integral method. The shape and period of oscillation are very close to that of Lundgren & Mansour (1988).

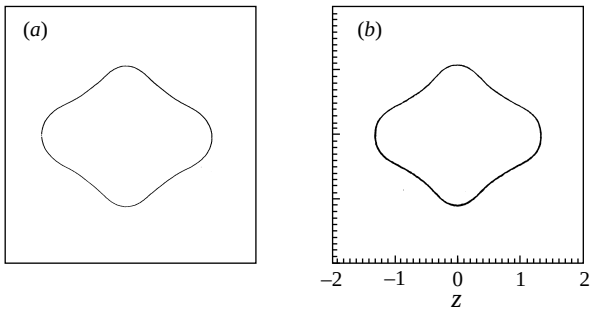

FIGURE 3. Comparison at $t = 1.1$ of the motion of an oscillating viscous drop in zero gravity computed using the level set method (*a*) and computed using the boundary integral method (*b*) of Lundgren & Mansour (1988). The drop is initialized with a P_4 shape with $\lambda = 0.01$, $\eta = 0.01$, $Re = 2000$, $We = 2$, and $Fr = \infty$.

4.2. *Rising gas bubble in a liquid*

4.2.1. *Steady-state results*

Hnat & Buckmaster (1976) conducted experiments with spherical-cap air bubbles rising in a liquid. The properties of the liquid and the gas are $\rho_\ell = 0.8755$ g cm^{-3}, $\rho_g = 0.001$ g cm^{-3}, $\mu_\ell = 1.18$ P, and $\mu_g = 0.01$ P. The coefficient of surface tension is $\sigma = 32.2$ dyn cm^{-1}. These experimental parameters give rise to the dimensionless quantities $\lambda = 0.0011$ and $\eta = 0.0085$.

In our numerical computations, the fluid domain is $\Omega = \{(r, z) | 0 \leqslant r \leqslant 3$ and $0 \leqslant z \leqslant 12\}$ and the grid size is 64×256. We use our far-field boundary conditions (see §2.6.3) in order to circumvent viscous wall effects. We shall compare our results with the experiments shown in figures 1A and 1C of Hnat & Buckmaster.

Bubble A We first examine the situation recorded in figure 1A of Hnat & Buckmaster where they observed that the steady rise speed of a gas bubble was 21.5 cm s^{-1}. Its volume was 0.94 cm^{-3} which gives an effective radius of 0.61 cm. This gives rise to the dimensionless quantities $Re = 9.8$, $Fr = 0.76$, and $We = 7.6$. The dimensionless rise speed should therefore be 1. We start with a spherical bubble of dimensionless radius one. In figure 4 we display the time evolution of the bubble. We observe that the bubble reaches a steady state with a final speed of 1.02 which corresponds to 21.9 cm s^{-1}. Figure 5 displays our computed rise speed of the bubble as function of time. The numerically computed speed and shape of the bubble are in agreement with the experimental observations of Hnat & Buckmaster. Our results are also in agreement with those of Ryskin & Leal (1984*b*, figure 6), who compute the same flow using a steady code.

Bubble C In figure 1C of Hnat & Buckmaster, a bubble of volume 5.2 cm^{-3} was observed to be moving with a steady speed of 30.5 cm s^{-1}. The effective radius was 1.08 cm. This gives rise to the dimensionless quantities $Re = 24.4$, $Fr = 0.88$, and $We = 27.2$. Our initial condition was a spherical bubble of dimensionless radius one. The time evolution of the bubble is displayed in figure 6. The bubble is seen to develop skirts which then break off, leaving behind a spherical-cap bubble rising at a constant speed. The steady rise speed in our computations was 29 cm s^{-1}, in close agreement with the observed value of 30.5 cm s^{-1}. The shape of the computed bubble also agreed with the findings of Hnat & Buckmaster. There is a difficulty, however, with making a direct comparison between this numerical computation and

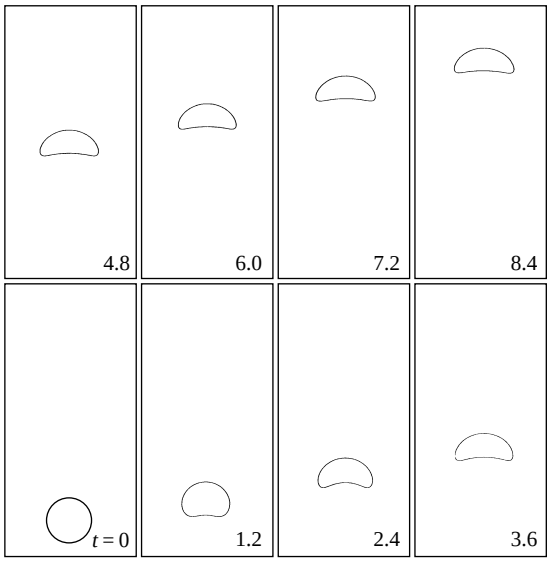

FIGURE 4. Evolution of a viscous gas bubble with $\lambda = 0.0011$, $\eta = 0.0085$, $Re = 9.8$, $We = 7.6$, and $Fr = 0.76$. This corresponds to bubble A of table I in Hnat & Buckmaster (1976).

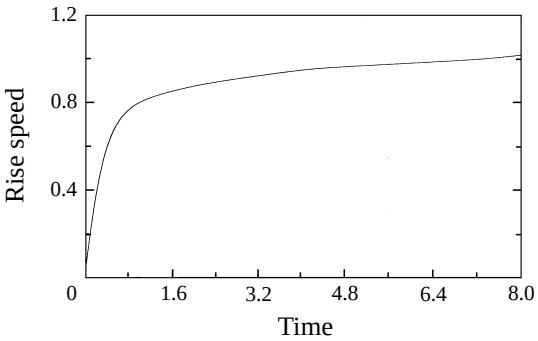

FIGURE 5. The time evolution of the velocity of the top of the bubble shown in figure 4.

the experimental results as the final bubble in our computation has a smaller volume than the bubble used in the experiment.

In the experiments of Hnat & Buckmaster, the volume was measured *after* the bubble had reached the top of the chamber instead of being measured initially. It is possible that the initial bubble could have developed thin skirts that eventually disintegrated into tiny air pockets, while the remainder of the bubble attained the steady-shape shown in figure 1C of Hnat & Buckmaster. To circumvent this difficulty, we allow the parameters, Re, We, and Fr, to vary linearly from the parameters of the Bubble A case ($t = 0$) to those of the Bubble C case ($t = 4$). Thus, we essentially start our bubble at $t = 4$ with a preset initial shape and velocity. In figure 7, we see that the results using our 'varying parameters' technique compare well with the experiments found in figure 1C of Hnat & Buckmaster. The final rise speed of our numerical computations was 29.5 cm s^{-1}.

Skirted bubbles Figure 8 shows an example of a skirted bubble which corresponds to $Re = 70$, $We = 115$, and $Fr = 99$. We start with a spherical gas bubble at

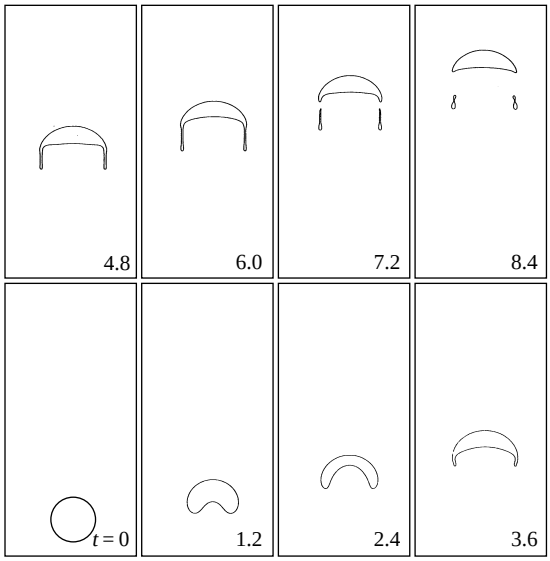

FIGURE 6. Evolution of a viscous gas bubble with $\lambda = 0.0011$, $\eta = 0.0085$, $Re = 24.4$, $We = 27.2$, and $Fr = 0.88$. This corresponds to bubble C of table I in Hnat & Buckmaster (1976).

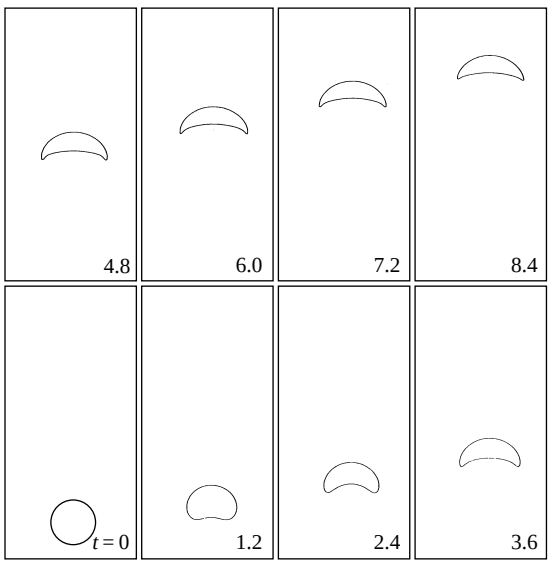

FIGURE 7. Evolution of a viscous gas bubble with $\lambda = 0.0011$, $\eta = 0.0085$, $Re = 24.4$, $We = 27.2$, and $Fr = 0.88$. This corresponds to bubble C of table I in Hnat & Buckmaster(1976). The initial data for this problem are the result at $t = 4.0$ of allowing a bubble to rise with the parameters of bubble A and then linearly varying Re, We, and Fr until they reach the parameters of bubble C at $t = 4.0$.

$t = 0$ and allow the parameters to vary, starting with the parameters of Bubble A, until $t = 4$. Our computed skirted bubble shares the basic features of the idealized skirted spherical-cap bubble shown in figure 2 of Hnat & Buckmaster. In addition, our computed skirted bubble has parameter values in the range where Hnat & Buckmaster observed skirted-cap bubbles.

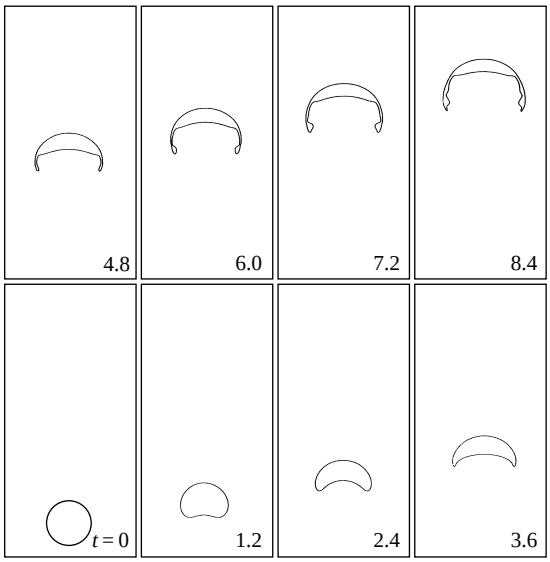

FIGURE 8. Evolution of a viscous gas bubble with $\lambda = 0.0011$, $\eta = 0.0085$, $Re = 70$, $We = 115$, and $Fr = 0.99$. The initial data for this problem are the result at $t = 4.0$ of allowing a bubble to rise with the parameters of bubble A and then varying Re, We, and Fr linearly until they reach the parameters given above at $t = 4.0$.

4.2.2. *Topology changes*

Ryskin & Leal (1984*a*,*b*) found that as the Reynolds and Weber numbers were increased they were unable to find steady rising bubble solutions using their method. This may be a result of the bubbles' tendency to undergo a topology change.

Lundgren & Mansour (1991) consider the time evolution of an initially spherical bubble. They take the bubble to be massless, incompressible and surrounded by an irrotational inviscid liquid ($Re = \infty$). Their calculation shows that if the surface tension is sufficiently small (We sufficiently large) the bottom surface of the bubble will collide with its upper surface.

We now consider the motion of an inviscid gas bubble rising in an inviscid liquid with $Fr = 1$, $B = 200$, and $Re = \infty$. In the boundary integral calculation we have $\lambda = 0$ with the liquid of infinite extent, whereas in the level set computation we take $\lambda = 0.001$ with the domain $\Omega = \{(r, z) | 0 \leqslant r \leqslant 4 \text{ and } 0 \leqslant z \leqslant 8\}$. We do not expect these differences to be responsible for any significant deviation between the two approaches. Our initial conditions consist of a spherical bubble with radius unity at rest in a quiescent fluid. We use 120×240 grid points for the level set computation and 120 points for the boundary integral method. We have also repeated the calculation for $B = 10$.

In figures 9 and 10, we display our results for Bond numbers, $B = 200$ and $B = 10$. Each figure compares the results of the boundary integral method to those of the level set method. The results are in close agreement with each other and with the results of Lundgren & Mansour(1991) until the time of the topology change. After the topology change the two different approaches are only in qualitative agreement. There are a number of possible reasons for the discrepancy, which are as follows:

(*a*) the 'surgery' performed in the boundary integral method is slightly inconsistent with a solution of the incompressible Euler equations;

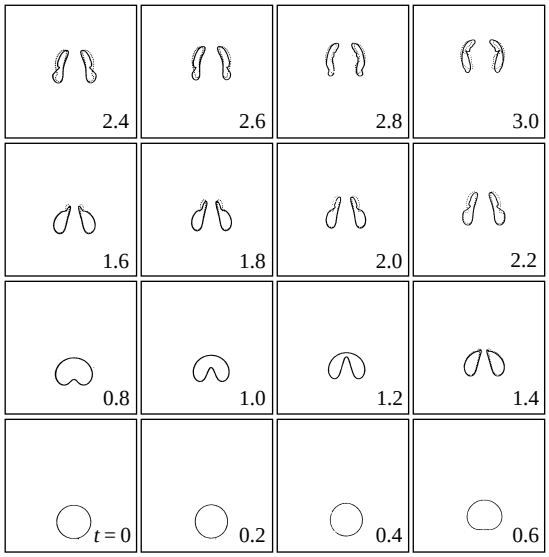

FIGURE 9. Evolution of an initially spherical gas bubble with $\lambda = 0.001$, $Re = \infty$, $B = 200$ and $Fr = 1$. The dashed lines represent the results from the boundary integral scheme and the solid lines represent the results from the level set method.

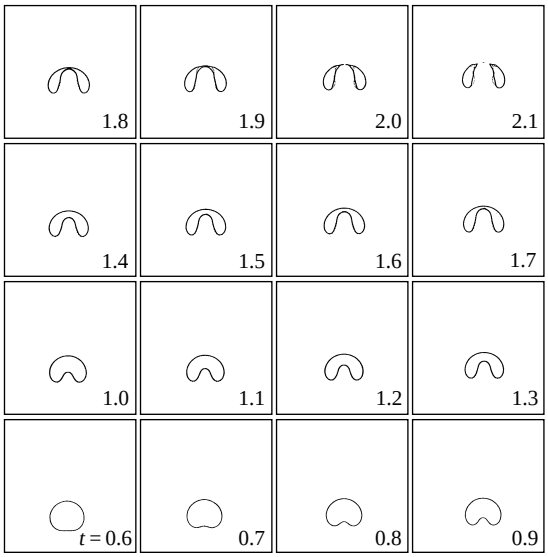

FIGURE 10. Evolution of an initially spherical gas bubble with $\lambda = 0.001$, $Re = \infty$, $B = 10$ and $Fr = 1$. The dashed lines represent the results from the boundary integral scheme and the solid lines represent the results from the level set method.

(*b*) there is significant numerical viscosity of the level set method at the topology change;

(*c*) there is a loss of uniqueness of solutions through the topology change and each method picks its own different solution.

It is our feeling that (*a*) is probably the most significant source of the discrepancy. Nevertheless, we find the results encouraging. These calculations appear to confirm

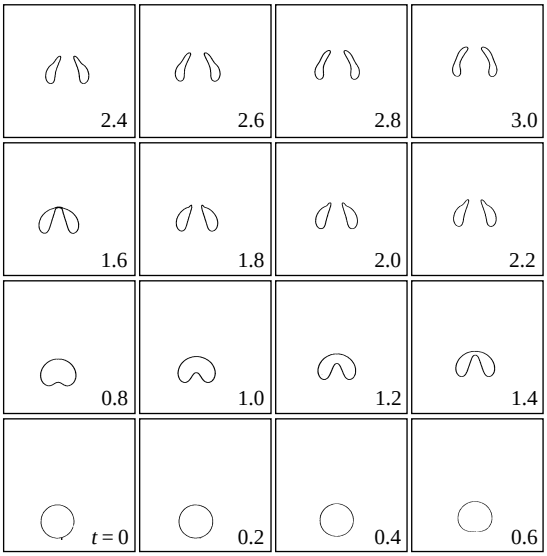

FIGURE 11. Evolution of an initially spherical gas bubble with $\lambda = 0.001$, $\eta = 0.01$, $Re = 100$, $B = 200$, and $Fr = 1$.

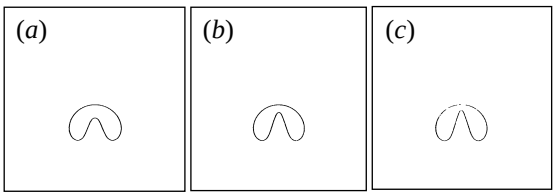

FIGURE 12. Comparison for various Reynolds numbers for the rising gas bubble problem with $\lambda = 0.001$, $\eta = 0.01$, $B = 200$, and $Fr = 1$ at $t = 1.2$. (*a*) $Re = 100$, (*b*) $Re = 400$, (*c*) $Re = \infty$.

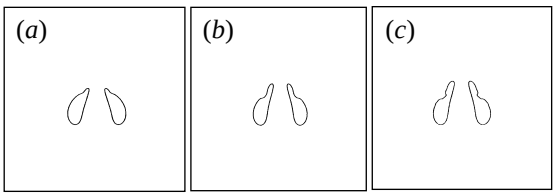

FIGURE 13. Comparison for various Reynolds numbers for the rising gas bubble problem with $\lambda = 0.001$, $\eta = 0.01$, $B = 200$, and $Fr = 1$ at $t = 2.0$. (*a*) $Re = 100$, (*b*) $Re = 400$, (*c*) $Re = \infty$.

the ideas developed by Benjamin & Ellis (1966) and Best (1993) concerning the formation of toroidal bubbles. The agreement between the level set method and the boundary integral method, prior to the topology change, indicates that the level set method has insignificant numerical viscosity for smooth interfaces.

In figures 11, 12, and 13, we demonstrate the effects of viscosity using our level set scheme. Figure 11 shows the same calculation as in figure 9 but for $Re = 100$. It is clear that the basic features have persisted with the inclusion of viscosity although the presence of viscosity has smoothed the bubble surface.

It is known (see Saffman 1956), for Reynolds numbers greater than 200, that inviscid bubble motion should closely approximate the viscous case. Our level set

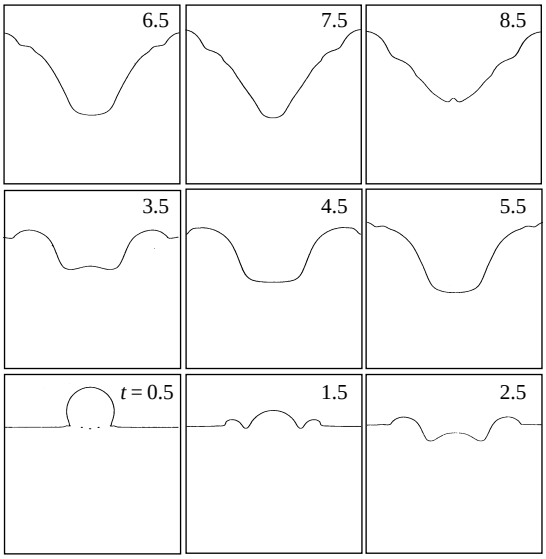

FIGURE 14. Evolution of a drop impinging on a water surface with $\lambda = 0.001$, $Re = \infty$, $Fr = 26.12$, and $We = 21.95$. This corresponds, approximately, to a 2.5 mm water drop hitting the water surface at 0.8 m s^{-1}.

computations are consistent with this result even after the topology change. Our results for $Re = 400$ are very close to that for the inviscid case, whereas for $Re = 100$ the effects of viscosity start to become noticeable (see figures 12, and 13).

4.3. *Water drop impinging on a pool of water*

Oguz & Prosperetti (1990) used a boundary integral scheme to compute the motion of an air–water free boundary after the impact of a raindrop. For initial conditions they took the drop to be already attached to the surface. They also compared their numerical results to the experimental observations of Pumphrey & Crum (1988) and found good agreement. Both studies found that the raindrop can cause a small air bubble to be entrained below the water surface. The air bubble entrainment was found to depend on the size and velocity of the raindrop. For example, if the drop is moving either too fast or too slow it will not entrain an air bubble. Oguz & Prosperetti found excellent quantitative agreement with Pumphrey & Crum on the drop size and velocity needed for entrainment. The entrained air bubble is thought to be an important source of underwater rain noise.

We also studied this problem using the level set method; unfortunately, we could not compute on a large enough domain to compare quantitatively with the results of Pumphrey & Crum (1988) and Oguz & Prosperetti (1990). We also found that the far-field boundary conditions did not work because the velocity field did not decay fast enough in space. Nevertheless, we obtained good qualitative agreement and we were able to compute past the time at which the bubble was entrained. The domain for our numerical computations is $\Omega = \{(r, z)0 \leqslant r \leqslant 3.8 \text{ and } 0 \leqslant z \leqslant 7.6\}$ with a 63×126 grid; we take $\lambda = 0.001$ and $\eta = 0.01$. We start our computations with a drop suspended just above the surface, and an initial gravitational force chosen such that the impact velocity is the proper dimensionless value at $t = 0.2$. For $t > 0.2$ the gravitational force is reset back to its proper value.

In figure 14 we present a calculation with $Re = \infty$, $Fr = 26.12$, and $We = 21.95$.

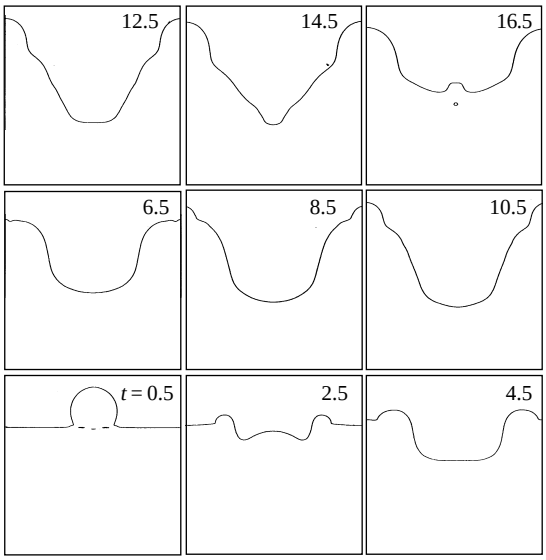

FIGURE 15. Evolution of a drop impinging on a water surface with $\lambda = 0.001$, $Re = \infty$, $Fr = 58.77$, and $We = 49.38$. This corresponds, approximately, to a 2.5 mm water drop hitting the water surface at 1.2 m s^{-1}.

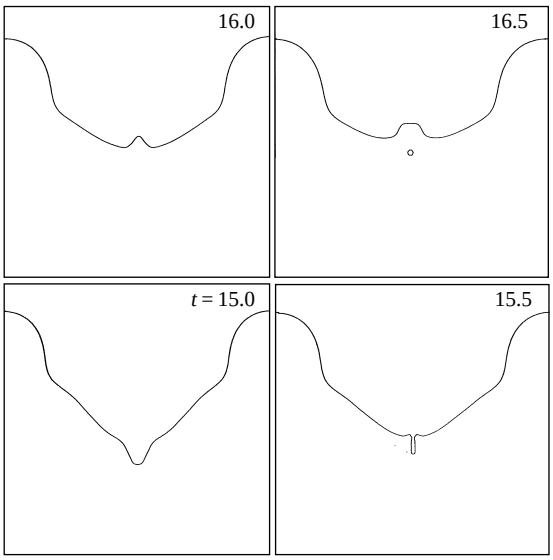

FIGURE 16. A detail of figure 15.

This corresponds to a 2.5 mm water drop hitting the water surface at 0.8 m s^{-1}. At impact we see tiny air bubbles trapped in the water which later break up into bubbles too small to be resolved. The subsequent motion of the water fails to entrain an air bubble. In figure 15 we present a calculation with $Re = \infty$, $Fr = 58.77$, and $We = 49.38$. This corresponds to a 2.5 mm water drop hitting the water surface at 1.2 m s^{-1}. In this case we see that an air bubble is entrained in a similar fashion to that shown by Oguz & Prosperetti (1990). Figure 16 shows the details of the air bubble entrainment.

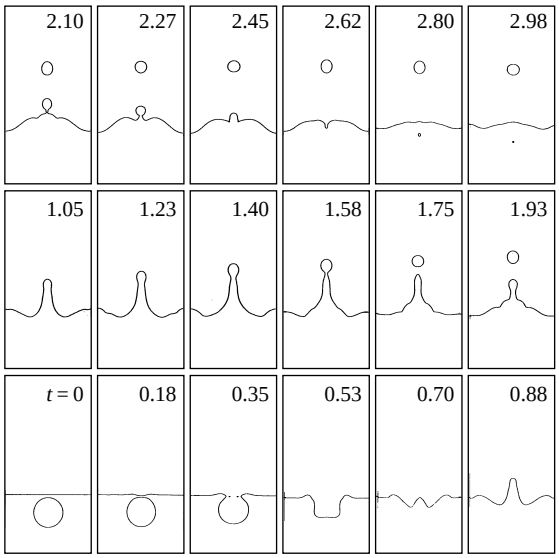

FIGURE 17. Evolution of a water jet resulting from a submerged gas bubble. $\lambda = 0.001$, $\eta = 0.01$, $Re = 474$, $We = 1$, and $Fr = 0.64$. This corresponds to an air bubble of radius 4 mm in water.

4.4. *Gas bubble bursting at a free surface*

Next we turn to the problem of a gas bubble rising to the free surface of a liquid. When the bubble breaks through the surface, large surface tension forces are produced which ultimately cause a jet of liquid to be ejected. This jet of liquid can subsequently break up into drops.

This problem was studied by Boulton-Stone & Blake (1993) using the boundary integral method with two different types of initial conditions. In one case, they consider a bubble that has already risen to the surface and is in static equilibrium before it bursts; this is called the 'pre-burst' case. They also considered the initial condition whereby a spherical bubble bursts at the surface. They found a considerable difference between the results for two initial conditions.

In our calculation, we consider a spherical gas bubble released just below the surface. We shall consider two situations which correspond to 4 and 5 mm air bubbles in water. The domain is $\Omega = \{(r, z) | 0 \leqslant r \leqslant 3 \text{ and } 0 \leqslant z \leqslant 12\}$ and the mesh is 44×176. For these computations we have $\lambda = 0.001$, $\eta = 1$, and $We = 1$. For the 4 mm gas bubble $Re = 474$ and $Fr = 0.64$; for the 5 mm gas bubble $Re = 531$ and $Fr = 0.29$. As the size of the bubble is reduced, the numerical problem becomes stiff. Since our method is explicit, extremely small time steps become necessary. Due to limited computing resources, we were unable to consider bubbles smaller than 4 mm and we were unable to compute on a large enough domain. This makes a quantitative comparison with Boulton-Stone & Blake (1993) impossible.

Our results, nevertheless, share many features predicted by their work; these results are shown in figures 17 and 18. In each case, we observe a jet of liquid ejected from the surface which is very similar to the results shown in figure 6 of Boulton-Stone & Blake (1993). The level set formulation allows us to continue the computation beyond the point where the liquid jet starts to break up into drops. The velocity of the liquid jet is plotted in figure 19. This graph is in reasonable agreement to the results displayed in figure 6 of Boulton-Stone & Blake despite the fact that their results were for a bubble of 3 mm. When comparing the jet speed for differently sized

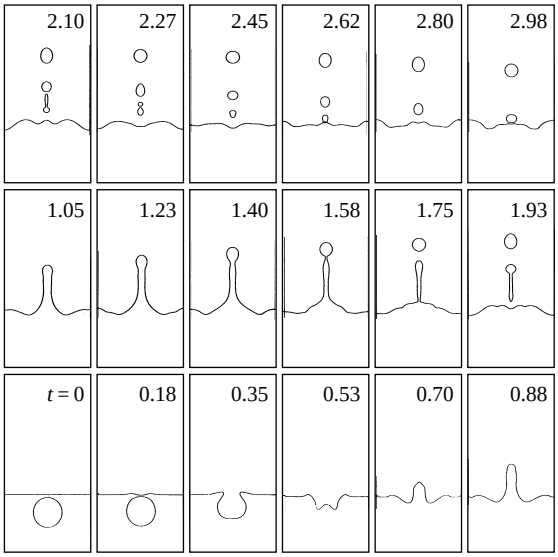

FIGURE 18. Evolution of a water jet resulting from a submerged gas bubble. $\lambda = 0.001$, $\eta = 0.01$, $Re = 531$, $We = 1$, and $Fr = 0.29$. This corresponds to an air bubble of radius 5 mm in water.

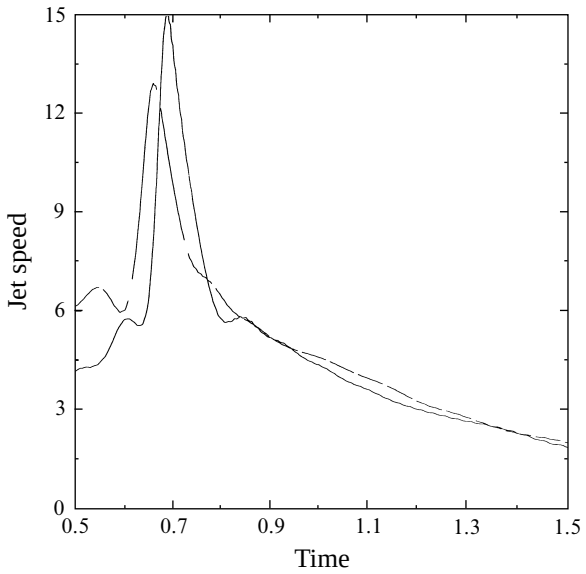

FIGURE 19. The jet speed for figures 17 and 18. The solid line is for the 4 mm bubble and the dashed line is for the 5 mm bubble.

initial bubbles, we find that smaller bubbles yield a larger jet speed which was also observed by Boulton-Stone & Blake.

5. Conclusion

We have presented an Eulerian scheme for computing a general incompressible flow on an axisymmetric domain. We have shown good agreement with the boundary

integral method, in spite of the difficulties due to the instabilities of inviscid flow and surface tension effects. Furthermore, we have demonstrated the ability to compute flow beyond interfacial singularities such as fluid entrapment and fragmentation. In the future, we would like to take advantage of adaptive mesh technology in order to better resolve the fine scale features of air/water flow.

The authors thank Brenda Brown for reading over the manuscript. The research for this work was started in the Department of Mathematics at the University of California, Los Angeles where it was supported in part by the Army Research Office, grant # DAAL03-91-G-0162. The first author's research at the Lawrence Livermore National Laboratory was performed under the auspices of the US Department of Energy by the Lawrence Livermore National Laboratory under contract No. W-7405-Eng-48. Support under contract No. W-7405-Eng-48 was provided by the Applied Mathematical Sciences Program of the Office of Energy Research. The second author was also supported by the National Science Foundation through a postdoctoral fellowship.

REFERENCES

Baker, G. R, Meiron, D. I. & Orszag, S. A. 1984 Boundary integral methods for axisymmetric and three-dimensional Rayleigh-Taylor instability problems. *Physica* **12D**, 19–31.

Bell, J. B., Colella, P. & Glaz, H. M. 1989 A second-order projection method for the incompressible Navier–Stokes equations. *J. Comput. Phys.* **85**, 257–283.

Benjamin, T. B. 1987 Hamiltonian theory for motions of bubbles in an infinite liquid. *J. Fluid Mech.* **181**, 349–379.

Benjamin, T. B. & Ellis, A. T. 1966 The collapse of cavitation bubbles and the pressures thereby produced against solid boundaries. *Phil. Trans. R. Soc. Lond.* A **260**, 221–240.

Best, J. P. 1993 The formation of toroidal bubbles upon the collapse of transient cavities. *J. Fluid Mech.* **251**, 79–107.

Best, J. P. 1994 The rebound of toroidal bubbles. In *Proc. IUTAM Symp. on Bubble Dynamics and Interface Phenomena* (ed. J. R. Blake, J. M. Boulton-Stone & N. H. Thomas), pp. 405–412.

Best, J. P. & Kucera, A. 1992 A numerical investigation of non-spherical rebounding bubbles. *J. Fluid Mech.* **245**, 137–154.

Blake, J. R. & Gibson, D. C. 1987 Cavitation bubbles near boundaries. *Ann. Rev. Fluid Mech.* **19**, 99–123.

Blake, J. R., Taib, B. B. & Doherty, G. 1986 Transient cavities near boundaries. Part 1. Rigid boundary. *J. Fluid Mech.***170**, 479–497.

Boulton-Stone, J. M. & Blake, J. R. 1993 Gas bubbles bursting at a free surface. *J. Fluid Mech.* **254**, 437–466.

Brackbill, J. U., Kothe, D. B. & Zemach, C. 1992 A continuum method for modeling surface tension. *J. Comput. Phys.* **101**, 335–353.

Chang, Y. C., Hou, T. Y., Merriman, B. & Osher, S. 1995 A level set formulation of Eulerian interface capturing methods for incompressible fluid flows. *J. Comput. Phys.*, submitted.

Dandy, D. S. & Leal, L. G. 1989 Buoyancy-driven motion of a deformable drop through a quiescent liquid at intermediate Reynolds numbers. *J. Fluid Mech.* **208**, 161–192.

Evans, L. C. & Spruck, J. 1991 Motion of level sets by mean curvature. I *J. Diffl Geom.* **33**, 635–681.

Fatemi, E. & Sussman, M. 1995 An efficient, interface preserving level set redistancing algorithm and its application to interfacial incompressible fluid flow. *SIAM J. Sci. Statist. Comput.*, submitted.

Hnat, J. G. & Buckmaster, J. D. 1976 Spherical cap bubbles and skirt formation. *Phys. Fluids* **19**, 182–194.

Jan, Y. J. & Tryggvason, G. 1994 A computational study of contaminated bubbles. Preprint.

Lamb, H. 1932 *Hydrodynamics*, 6th edn. Cambridge University Press.

Longuet-Higgins, M. S. & Cokelet, E. D. 1976 The deformation of steep surface waves on water. I A numerical method of computation. *Proc. R. Soc. Lond.* A **350**, 1–26.

Lundgren, T. S. & Mansour, N. N. 1988 Oscillations of drops in zero gravity with weak viscous effects. *J. Fluid Mech.* **194**, 479–510.

Lundgren, T. S. & Mansour, N. N. 1991 Vortex ring bubbles. *J. Fluid Mech.* **224**, 177–196.

Miksis, M. J., Vanden-Broeck, J.-M. & Keller, J. B. 1982 Rising bubbles. *J. Fluid Mech.* **123**, 31–41.

Mulder, W., Osher, S. & Sethian, J. A. 1992 Computing interface motion in compressible gas dynamics. *J. Comput. Phys.* **100**, 209–228.

Nobari, M. R. & Tryggvason, G. 1994 Numerical simulations of drop collisions. *AIAA* 94-0835.

Oguz, H. N. & Prosperetti, A. 1990 Bubble entrainment by the impact of drops on liquid surfaces. *J. Fluid Mech.* **203**, 143–179.

Osher, S. & Sethian, J. A. 1988 Fronts propagating with curvature-dependent speed: algorithms based on Hamilton-Jacobi formulations. *J. Comput. Phys.* **79**, 12–49.

Pumphrey, H. C. & Crum, L. A. 1988 Acoustic emissions associated with drop impacts. In *Natural Mechanisms of Surface-Generated Noise in the Ocean* (ed. B.R. Kerman), pp. 463–483. Reidel.

Ryskin, G. & Leal, L. G. 1984*a* Numerical solution of free boundary problems in fluid mechanics. Part 1. The finite-difference technique. *J. Fluid Mech.* **148**, 1–17.

Ryskin, G. & Leal, L. G. 1984*b* Numerical solution of free boundary problems in fluid mechanics. Part 2. Buoyancy-driven motion of a gas bubble through a quiescent liquid. *J. Fluid Mech.* **148**, 19–35.

Saffman, P. G. 1956 On the rise of small bubbles in water. *J. Fluid Mech.* **1**, 249–275.

Shu, C. W. & Osher, S. J. 1989 Efficient implementation of essentially nonoscillatory shock capturing schemes II. *J. Comput. Phys* **83**, 25–37.

Sussman, M. 1994 A level set approach for computing solutions to incompressible two-phase flow. Thesis, University of California, Los Angeles.

Sussman, M., Smereka, P. & Osher, S. J. 1994 A level set approach for computing solutions to incompressible two-phase flow. *J. Comput. Phys.* **114**, 146–159 (referred to herein as Paper I).

Szymczak, W. G., Rogers, J., Solomon, J. M. & Berger, A. E. 1993 A numerical algorithm for hydrodynamic free boundary problems. *J. Comput. Phys.* **106**, 319–336.

Thorsen, G., Stordalen, R. M. & Terjesen, S. G. 1968 On the terminal velocity of circulating and oscillating liquid drops. *Chem. Engng Sci.* **23**, 413–426.

Unverdi, S. O. & Tryggvason, G. 1992 A front-tracking method for viscous, incompressible, multi-fluid flows. *J. Comput. Phys.* **100**, 25–37.

Zhang, S., Duncan, J. H. & Chahine, G. L. 1993 The final stage of the collapse of a cavitation bubble near a rigid wall. *J. Fluid Mech.* **257**, 147–181.